

Marquette University

e-Publications@Marquette

---

Chemistry Faculty Research and Publications

Chemistry, Department of

---

2018

## From Static to Dynamic: Electron Density of HOMO at Biaryl Linkage Controls the Mechanism of Hole Delocalization

Maxim V. Ivanov  
*Marquette University*

Denan Wang  
*Marquette University*

Rajendra Rathore  
*Marquette University*, [rajendra.rathore@marquette.edu](mailto:rajendra.rathore@marquette.edu)

Follow this and additional works at: [https://epublications.marquette.edu/chem\\_fac](https://epublications.marquette.edu/chem_fac)

 Part of the [Chemistry Commons](#)

---

### Recommended Citation

Ivanov, Maxim V.; Wang, Denan; and Rathore, Rajendra, "From Static to Dynamic: Electron Density of HOMO at Biaryl Linkage Controls the Mechanism of Hole Delocalization" (2018). *Chemistry Faculty Research and Publications*. 877.

[https://epublications.marquette.edu/chem\\_fac/877](https://epublications.marquette.edu/chem_fac/877)

Marquette University

e-Publications@Marquette

***Chemistry Faculty Research and Publications/College of Arts and Sciences***

***This paper is NOT THE PUBLISHED VERSION; but the author's final, peer-reviewed manuscript.*** The published version may be accessed by following the link in the citation below.

*Journal of the American Chemical Society*, Vol. 140, No. 14 (2018): 4765-4769. [DOI](#). This article is © American Chemical Society and permission has been granted for this version to appear in [e-Publications@Marquette](#). American Chemical Society does not grant permission for this article to be further copied/distributed or hosted elsewhere without the express permission from American Chemical Society.

## From Static to Dynamic: Electron Density of HOMO at Biaryl Linkage Controls the Mechanism of Hole Delocalization

Maxim V. Ivanov

Department of Chemistry, Marquette University, Milwaukee, WI

Denan Wang

Department of Chemistry, Marquette University, Milwaukee, WI

Rajendra Rathore

Department of Chemistry, Marquette University, Milwaukee, WI

### Abstract

In order to extend the physical length of hole delocalization in a molecular wire, chromophores of increasing size are often desired. However, the effect of size on the efficacy and mechanism of hole delocalization remains elusive. Here, we employ a model set of biaryls to show that with increasing chromophore size, the mechanism of steady-state hole distribution switches from static delocalization in biaryls with smaller chromophores to dynamic hopping, as exemplified in the largest system, <sup>tBu</sup>HBC<sub>2</sub> (i.e., “superbiphenyl”), which displays a vanishingly small electronic coupling. This important finding is analyzed with the aid of Hückel molecular orbital and Marcus–Hush theories. Our findings will enable

the rational design of the novel molecular wires with length-invariant redox/optical properties suitable for long-range charge transfer.

Development of a thorough understanding of all critical elements controlling the extent of charge delocalization in molecular wires is essential for the rational design of long-range charge-transfer materials.<sup>1-4</sup> Studies of poly-*p*-phenylene-based wires have shown<sup>5-9</sup> that the cationic charge (i.e., hole) delocalization is limited to  $\sim 8$  *p*-phenylene units (or  $\sim 3$  nm), as evidenced by an abrupt saturation of their redox/optical properties, i.e., a breakdown of the  $\cos[\pi/(n + 1)]$  (or  $1/n$ ) dependence<sup>9-11</sup> observed for  $n > 8$ . Such limited hole delocalization arises from the interplay between the energetic gain from hole delocalization and the penalty of structural/solvent reorganization.<sup>8,9</sup>

In order to extend the physical length of hole delocalization, one may exploit molecular wires with size of chromophore that is larger than a single phenylene, such as fluorene, hexabenzocoronene (**HBC**), or a novel **HBC**–fluorene hybrid<sup>12</sup> (**FHBC**), as shown on the example of representative wires with varied chromophore size in Figure 1. In fact, such a strategy has been extensively explored with porphyrin-based molecular wires that exhibit the largest hole delocalization lengths among common conjugated polymers.<sup>13-17</sup>

As another model system, a molecular wire with **HBCs** as chromophores is roughly by a factor of 3 longer than simple poly-*p*-phenylene (Figure 1), yet bears similar structural properties. Indeed, **HBC**-based biaryl (i.e., “superbiphenyl”)<sup>18</sup> is expected to undergo a free rotation with an equilibrium interplanar angle of  $\sim 30^\circ$ , akin to a simple biphenyl,<sup>19</sup> as illustrated below:

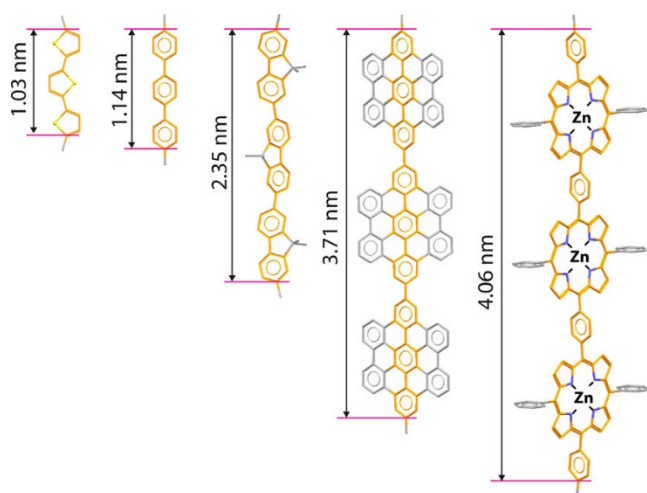
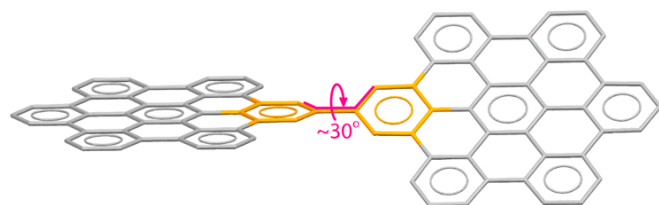


Figure 1. Molecular wires with varied chromophore size.



A series of recent studies<sup>20–22</sup> have shown that besides the geometrical requirement of a small interplanar angle, the frontier orbitals overlap, and their nodal arrangement are critically important for promoting a large electronic coupling. In this context, it thus remains unclear what impact the size of the chromophore has on the electronic structure of a chromophore and the associated electronic coupling.

In order to probe this key issue, we undertook a detailed analysis of the electronic structure of the biaryls with varied chromophore size, i.e., simple biphenyls with varied substituents ( $R\text{PP}_2$ ), bifluorene ( $F_2$ ), bitriphenylene ( $t\text{BuTP}_2$ ), and HBC-based biaryl (i.e.,  $t\text{BuHBC}_2$ ). We show that the increase of the chromophoric size reduces the interchromophoric electronic coupling and can switch the mechanism of hole distribution from static delocalization, characteristic for biphenyl cation radicals,<sup>23,24</sup> to dynamic hopping, as evidenced by electrochemical analysis, steady-state electronic absorption spectroscopy, and density functional theory (DFT) calculations. This important realization of the structure–function relationship may prove to be important in the rational design of novel charge-transfer materials.

Biphenyls ( $R\text{PP}_2$ ) with substituent  $R = H$ , isoalkyl ( $iA$ ), alkoxy ( $AO$ ), dialkylamino ( $iA2N$ ), and bifluorene ( $F_2$ ) were readily available,<sup>8,9,25</sup> while  $t\text{BuTP}_2$  and  $t\text{BuHBC}_2$  were synthesized by adaptation of standard literature procedures.<sup>26,27</sup> All compounds were characterized by  $^1\text{H}/^{13}\text{C}$  NMR spectroscopy and MALDI mass spectrometry. See Supporting Information for full details.

Electrochemical analysis of  $R\text{PP}_2$  showed that with increasing donor strength of the substituent, the hole stabilization (i.e.,  $\Delta E_{\text{ox}} = E_{\text{ox}}[\text{biaryl}] - E_{\text{ox}}[\text{aryl}]$ ) decreases from  $\Delta E_{\text{ox}} = -700$  mV in  $R = H$  to  $\Delta E_{\text{ox}} = -450$  mV in  $R = iA2N$  (Figure 2).

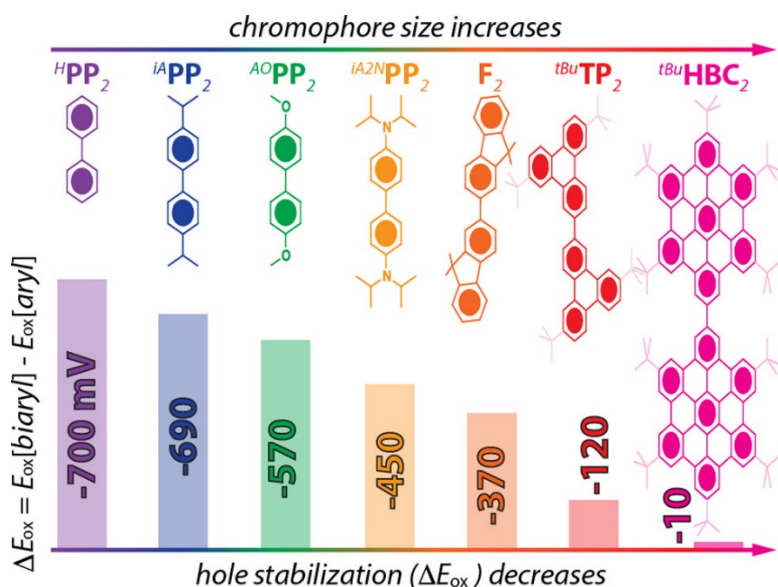


Figure 2. Hole stabilization ( $\Delta E_{\text{ox}}$ ) in biaryls as compared to monoaryl with varied size of the aryl chromophore.

Interestingly, expansion of the aryl core from a single benzenoid unit in  $H\text{PP}_2$  ( $\Delta E_{\text{ox}} = -700$  mV) to two benzenoids in  $F_2$  ( $\Delta E_{\text{ox}} = -370$  mV) to three benzenoids in  $t\text{BuTP}_2$  ( $\Delta E_{\text{ox}} = -120$  mV) reduces hole

stabilization by almost 0.6 V (Figure 2). To our surprise, further increasing the size of the chromophore to seven benzenoid rings, i.e., in  ${}^{tBu}\mathbf{HBC}_2$ , almost completely inhibits hole stabilization (i.e.,  $\Delta E_{ox} = -10$  mV)!

Electronic absorption spectra of biaryl cation radicals show that the characteristic near-IR band, absent in the corresponding monomers (Figure S15 in the Supporting Information), shifts to lower energy (longer wavelength) in going from  ${}^H\mathbf{PP}_2^{+\bullet}$  to  ${}^{tBu}\mathbf{TP}_2^{+\bullet}$  (Figure 3A). This indicates that, while the hole is delocalized over both chromophores (i.e., Robin-Day class III),<sup>28</sup> the electronic coupling decreases. Although a structured near-IR band is present in both  ${}^{tBu}\mathbf{HBC}^{+\bullet}$  and  ${}^{tBu}\mathbf{HBC}_2^{+\bullet}$ , the spectrum of  ${}^{tBu}\mathbf{HBC}_2^{+\bullet}$  bears no apparent additional features in comparison with that of  ${}^{tBu}\mathbf{HBC}^{+\bullet}$  (Figure 3B), suggesting that in  ${}^{tBu}\mathbf{HBC}_2^{+\bullet}$  the hole resides on a single chromophore (i.e., Robin-Day class I/II), consistent with the (steady-state) dynamic hole hopping mechanism.<sup>24,28</sup>

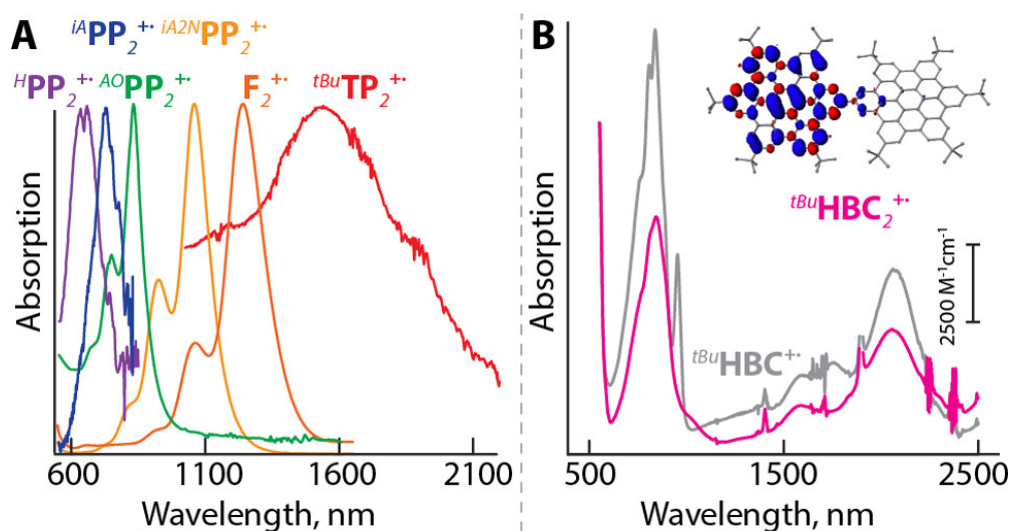


Figure 3. (A) Electronic absorption spectra of biaryl cation radicals. See Supporting Information for details of their generation. (B) Electronic absorption spectra of  ${}^{tBu}\mathbf{HBC}^{+\bullet}$  and  ${}^{tBu}\mathbf{HBC}_2^{+\bullet}$ . Isovalue plot of the spin-density distribution in  ${}^{tBu}\mathbf{HBC}_2^{+\bullet}$  shows hole localization on one  $\mathbf{HBC}$  unit.

DFT calculations of the oxidation and excitation energies of the biaryl cation radicals, computed at the benchmarked<sup>25,29</sup> (TD)-B1LYP-40/6-31G(d)+PCM(CH<sub>2</sub>Cl<sub>2</sub>) level of theory, showed a perfect agreement with the experimental data (Figure S14 in the Supporting Information). Natural population analysis<sup>30</sup> further confirmed that in all biaryls, except  ${}^{tBu}\mathbf{HBC}_2^{+\bullet}$ , the spin/charge and structural reorganization are delocalized over both chromophores (Figure S31 in the Supporting Information).

Electrochemical data, together with the analysis of the steady-state spectroscopic signatures and DFT calculations, suggest that as the size of the chromophore in biaryls increases, the electronic coupling decreases. In the extreme case of  ${}^{tBu}\mathbf{HBC}_2^{+\bullet}$ , this leads to a switch-over of the mechanism of hole distribution from static delocalization to dynamic hopping, akin to the one observed for biaryls with varied interplanar dihedral angle.<sup>24</sup> In order to rationalize this finding, we now analyze the electronic

structure of neutral and cation radicals of the biaryls with varied substitution and chromophore size in the context of Hückel molecular orbital and Marcus–Hush theories.

Following Hückel's method of representing molecular orbitals as a linear combination of  $p_z$  orbitals in  $\pi$ -conjugated hydrocarbons,<sup>31</sup> MOs in a biaryl can be represented as a linear combination of the HOMO of a single aryl (Figure 4).

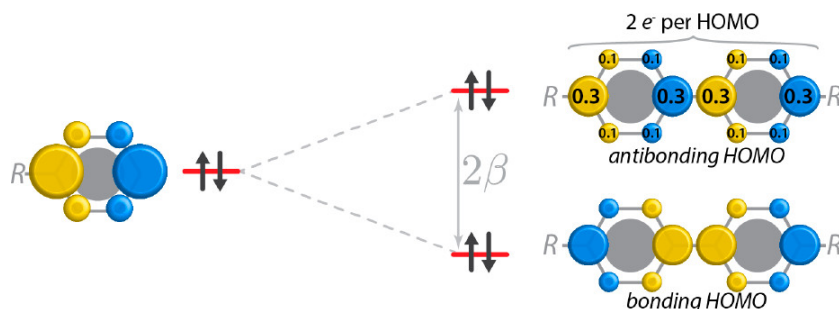


Figure 4. Molecular orbital diagram of a biaryl. Size of the circle represents the amount of electron density of HOMO at each atom as quantified by the Mulliken population analysis on the example of  ${}^H\text{PP}_2$ .

In a simple  ${}^H\text{PP}_2$ , the HOMO electron density is shared between 12 carbons, with the largest density residing along four middle carbons (as quantified<sup>32</sup> by a Mulliken population analysis) due to the longitudinal arrangement of the bisallylic HOMO (Figure 4). The high density at the biaryl linkage together with a relatively small interplanar dihedral angle of  $\sim 35^\circ$  result in a significant overlap between HOMOs of two aryls in  ${}^H\text{PP}_2$  and a large electronic coupling ( $\beta = 0.75$  eV) as measured by the HOMO/HOMO–1 energy gap (Figure 4).

As the donor strength of the substituent in  ${}^R\text{PP}_2$  increases, electron density of HOMO redistributes toward electron rich atoms of the substituent (Table S4 in the Supporting Information), thereby decreasing the HOMO density at the pair of carbons that mediate the electronic coupling through the biaryl linkage (Figure 5). A stronger effect can be achieved by increasing the size of the chromophore, where a total of two electrons per HOMO, in each case, spreads over a larger number of atoms, leading to a depleted per-atom electron density (Figure 5). Although Mulliken approximation states that electronic coupling is proportional to the orbital overlap,<sup>33–35</sup> the magnitude of the overlap also depends on the available electron density at a given atom, and thus, reduced HOMO electron density is expected to reduce the electronic coupling.

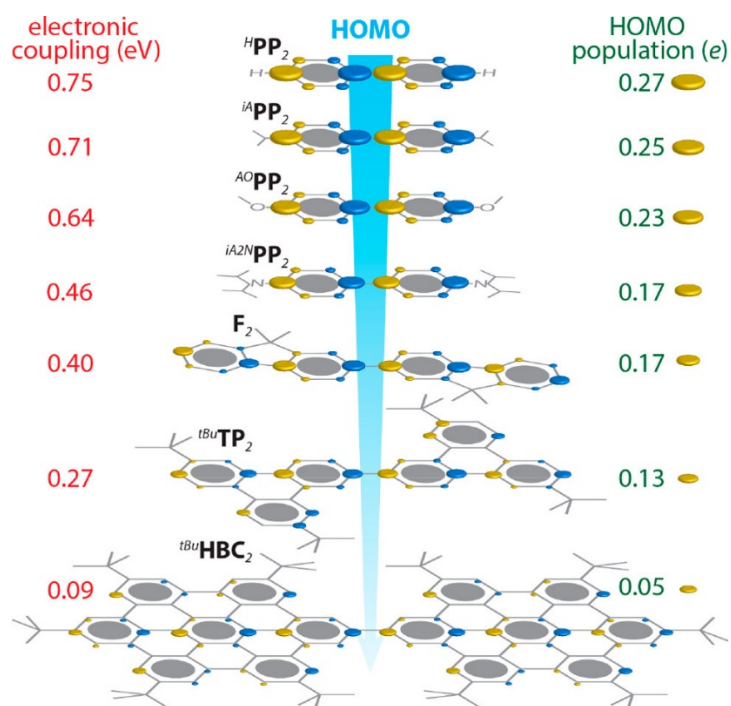


Figure 5. Schematic illustration of the HOMOs of various biaryls. See Figures S18–S24 in the Supporting Information for actual HOMO plots.

Mulliken population analysis of the HOMO density matrix reveals that the HOMO population at the center carbon ( $q_c$ ) and the magnitude of the overlap population between two monoaryl fragments ( $|S_{ab}|$ , see section S4.4. in the Supporting Information for details) both sharply decrease when going from  $HPP_2$  to  $tBuHBC_2$  (Figure 5). Furthermore, reduction of the HOMO electron density at the carbons forming biaryl linkage (either by using better electron donors as substituents or by expanding the size of the chromophore) is accompanied by a linear decrease in the electronic coupling (Figure 6A). In particular, changing the substituent in  $RPP_2$  from  $H$  to  $iA2N$  reduces the electronic couplings from 0.75 to 0.46 eV (Figure 6B), while doubling of the chromophore size from single phenylene to fluorene (i.e.,  $HPP_2$  vs  $F_2$ ) almost proportionally reduces the electronic coupling from 0.75 to 0.40 eV, and further expansion of the chromophore to 7 benzenoid rings in  $tBuHBC_2$  reduces the coupling to a negligible value of 0.09 eV (Figure 6B).

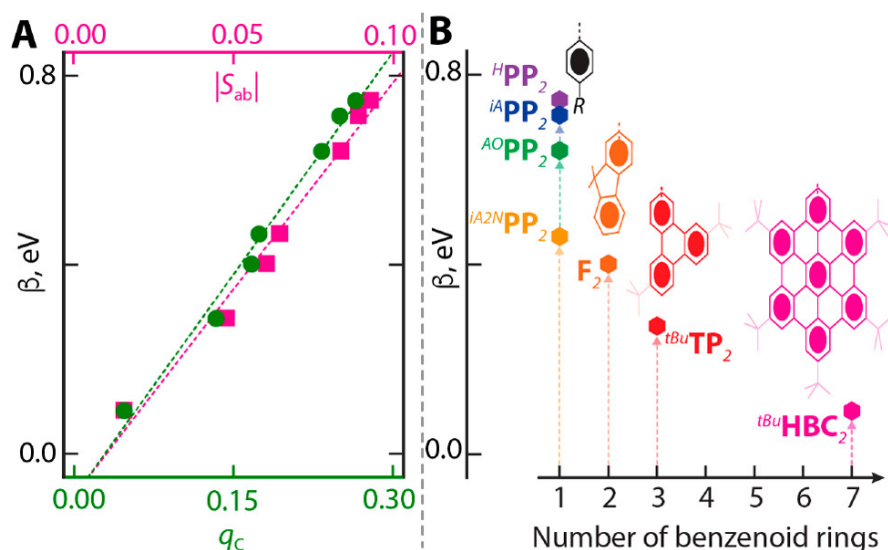


Figure 6. (A) Correlation plot between electronic coupling ( $\beta$ ) and HOMO population of the center carbons  $q_c$  (green circles) forming biaryl linkage and between  $\beta$  and the magnitude of overlap population  $|S_{ab}|$  (magenta squares) calculated at B1LYP-40/6-31G(d)+PCM(CH<sub>2</sub>Cl<sub>2</sub>). (B) Plot between  $\beta$  and chromophore size of biaryls measured in the number of benzenoid rings.

The lowering of the electronic coupling ( $\beta$ ) with increasing donor strength of the substituent and/or chromophore size in biaryls is translated into a reduced biaryl hole stabilization in their cation radicals ( $\Delta E_{ox}$ ) as indicated by the linear relationship between  $\beta$  and  $\Delta E_{ox}$  (Figure S25B in Supporting Information). Summarizing, hole stabilization is the largest for a biaryl with the largest HOMO electron density at the carbons of the biaryl linkage, and it reduces as the number of atoms contributing to the HOMO increases in the chromophores.

While molecular orbital analysis of neutral biaryls provides an important connection between electronic coupling and the HOMO electron density distribution in biaryls, understanding the origin of hole localization in  $tBuHBC_2^{+\bullet}$  also requires consideration of structural/solvent reorganization.

We have recently shown<sup>24</sup> in a series of biaryls with varied interplanar dihedral angle ( $\varphi$ ) that the mechanism of hole distribution is determined by the interplay between the electronic coupling ( $H_{ab}$ ) and the structural/solvent reorganization energy ( $\lambda$ ). That is, starting from a planar biaryl, an increase in  $\varphi$  leads to a switch-over of the mechanism of hole delocalization from static delocalization, as indicated by a linear  $v_{abs}$  vs  $\cos(\varphi)$  dependence ( $2H_{ab} > \lambda$ , class III) to dynamic hopping, as indicated by the corresponding nonlinear dependence ( $2H_{ab} < \lambda$ , class II).

Application of this computational analysis to the series of biaryl cation radicals considered here reveals that as the chromophore size (and donor strength of the substituent in biphenyl) increases, the switch-over of the hole distribution mechanism occurs at smaller angles, due to the decreasing electronic coupling and increasing structural reorganization (Figure 7). The small equilibrium dihedral angles in  $RPP_2^{+\bullet}$ ,  $F_2^{+\bullet}$ , and  $tBuTP_2^{+\bullet}$  place these biaryls into a linear  $v_{abs}$  vs  $\cos(\varphi)$  regime, ensuring that the mechanism of hole delocalization is static delocalization (Figure 7). However, expanded chromophores

in  $tBuHBC_2^{+\bullet}$  lead to nearly nonexistent electronic coupling, with the reorganization energy being the largest among all biaryls (Table S10 in the Supporting Information), consistent with a dynamic hopping mechanism of hole distribution, even for fully planarized  $tBuHBC_2^{+\bullet}$  (Figure 7).

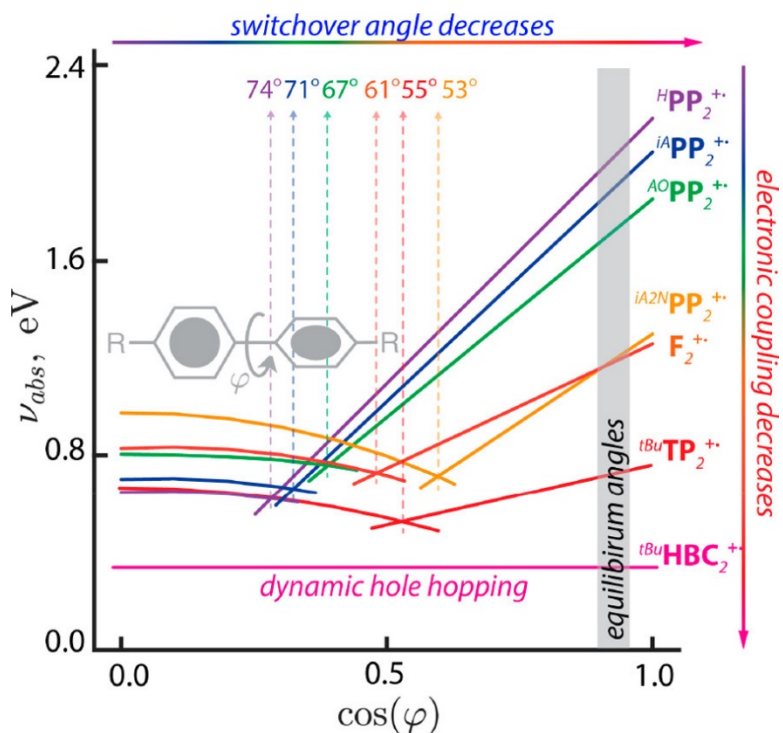


Figure 7. Interpolated plots of the TD-DFT [B1LYP-40/6-31G(d)+PCM(CH<sub>2</sub>Cl<sub>2</sub>)] excitation energy of various biaryl cation radicals (utilized in this study) against varied interplanar dihedral angles. Also see Figures S34–S40 in the Supporting Information for plots with actual data points.

In this communication, we have shown the effect of HOMO electron density at the biaryl linkage on the electronic coupling and hole distribution in a series of biaryls. Importantly, the control over the amount of HOMO electron density can be achieved either by a simple substitution in a parent biphenyl  $RPP_2$  or by increasing the size of the chromophore. As the donor strength of the substituent/chromophore size increases, the HOMO electron density at the coupling-mediating carbons of the biaryl linkage decreases, leading to a smaller orbital overlap and thereby smaller interchromophoric electronic coupling. In this context,  $tBuHBC_2$  with expanded graphitic cores of its chromophores represents an extreme case where the electronic coupling nearly vanishes, consistent with a dynamic hopping mechanism of steady-state hole distribution. One may envision that the **HBC**-based wires<sup>36,37</sup> would belong to the class of isoenergetic wires<sup>22,38</sup> with length-invariant redox/optical properties and therefore could be a potential candidate as a wire suitable for long-range charge transfer.<sup>39–42</sup> By combining the effects of the chromophore size and varied substitution, one can achieve a precise control over the electron density distribution in a chromophore and design novel charge-transfer materials with tailored redox and optoelectronic properties.

## Supporting Information

The Supporting Information is available free of charge on the ACS Publications website at DOI: 10.1021/jacs.8b00466.

Synthesis, electrochemistry, electronic spectroscopy of biaryl cation radicals, transient absorption spectroscopy, quantitative redox titrations, density functional theory calculations, computational details, redox/optical properties of biaryls, frontier orbital analysis, Mulliken population analysis of biaryls, structural analysis of the oxidation-induced bond-length changes in biaryls, influence of the geometrical parameters on the electronic coupling, and Marcus–Hush two-state model of biaryls.

## Acknowledgments

We thank the NSF (CHE-1508677) and NIH (R01-HL112639-04) for financial support, and Professor Scott A. Reid and Professor James R. Gardinier for helpful discussions. The calculations were performed on the high-performance computing cluster Pèrè at Marquette University and the Extreme Science and Engineering Discovery Environment (XSEDE).

## References

1. Ratner, M. *Nat. Nanotechnol.* 2013, 8, 378, DOI: 10.1038/nnano.2013.110
2. Guldi, D. M.; Nishihara, H.; Venkataraman, L. *Chem. Soc. Rev.* 2015, 44, 842, DOI: 10.1039/C5CS90010G
3. Lin, Y.; Zhan, X. *Acc. Chem. Res.* 2016, 49, 175, DOI: 10.1021/acs.accounts.5b00363
4. Mosquera, M. A.; Fu, B.; Kohlstedt, K. L.; Schatz, G. C.; Ratner, M. A. *ACS. Energy. Letters.* 2018, 3, 155, DOI: 10.1021/acsenergylett.7b01058
5. Takeda, N.; Miller, J. R. *J. Phys. Chem. B* 2012, 116, 14715, DOI: 10.1021/jp3096242
6. Ghosh, R.; Pochas, C.; Spano, F. *J. Phys. Chem. C* 2016, 120, 11394, DOI: 10.1021/acs.jpcc.6b02917
7. Zaikowski, L.; Kaur, P.; Gelfond, C.; Selvaggio, E.; Asaoka, S.; Wu, Q.; Chen, H.-C.; Takeda, N.; Cook, A. R.; Yang, A.; Rosanelli, J.; Miller, J. R. *J. Am. Chem. Soc.* 2012, 134, 10852, DOI: 10.1021/ja301494n
8. Wang, D.; Talipov, M. R.; Ivanov, M. V.; Rathore, R. *J. Am. Chem. Soc.* 2016, 138, 16337, DOI: 10.1021/jacs.6b09209
9. Ivanov, M. V.; Talipov, M. R.; Boddada, A.; Abdelwahed, S. H.; Rathore, R. *J. Phys. Chem. C* 2017, 121, 1552, DOI: 10.1021/acs.jpcc.6b12111
10. Torras, J.; Casanovas, J.; Alemán, C. *J. Phys. Chem. A* 2012, 116, 7571, DOI: 10.1021/jp303584b
11. Meier, H.; Stalmach, U.; Kolshorn, H. *Acta Polym.* 1997, 48, 379, DOI: 10.1002/actp.1997.010480905
12. Navale, T. S.; Ivanov, M. V.; Hossain, M. M.; Rathore, R. *Angew. Chem., Int. Ed.* 2018, 57, 790, DOI: 10.1002/anie.201711739
13. Peeks, M. D.; Tait, C. E.; Neuhaus, P.; Fischer, G. M.; Hoffmann, M.; Haver, R.; Cnossen, A.; Harmer, J. R.; Timmel, C. R.; Anderson, H. L. *J. Am. Chem. Soc.* 2017, 139, 10461, DOI: 10.1021/jacs.7b05386

14. Kuang, G.; Chen, S.-Z.; Wang, W.; Lin, T.; Chen, K.; Shang, X.; Liu, P. N.; Lin, N. *J. Am. Chem. Soc.* 2016, 138, 11140, DOI: 10.1021/jacs.6b07416
15. Rawson, J.; Angiolillo, P. J.; Therien, M. J. *Proc. Natl. Acad. Sci. U. S. A.* 2015, 112, 13779, DOI: 10.1073/pnas.1512318112
16. Parkinson, P.; Kondratuk, D. V.; Menelaou, C.; Gong, J. Q.; Anderson, H. L.; Herz, L. M. *J. Phys. Chem. Lett.* 2014, 5, 4356, DOI: 10.1021/jz5022153
17. Susumu, K.; Frail, P. R.; Angiolillo, P. J.; Therien, M. J. *J. Am. Chem. Soc.* 2006, 128, 8380, DOI: 10.1021/ja0614823
18. Ito, S.; Herwig, P. T.; Böhme, T.; Rabe, J. P.; Rettig, W.; Müllen, K. *J. Am. Chem. Soc.* 2000, 122, 7698, DOI: 10.1021/ja000850e
19. Johansson, M. P.; Olsen, J. *J. Chem. Theory Comput.* 2008, 4, 1460, DOI: 10.1021/ct800182e
20. Talipov, M. R.; Navale, T. S.; Rathore, R. *Angew. Chem., Int. Ed.* 2015, 54, 14468, DOI: 10.1002/anie.201506402
21. Ivanov, M. V.; Thakur, K.; Boddeda, A.; Wang, D.; Rathore, R. *J. Phys. Chem. C* 2017, 121, 9202, DOI: 10.1021/acs.jpcc.7b02264
22. Ivanov, M. V.; Chebny, V. J.; Talipov, M. R.; Rathore, R. *J. Am. Chem. Soc.* 2017, 139, 4334, DOI: 10.1021/jacs.7b01226
23. Erickson, R.; Lund, A.; Lindgren, M. *Chem. Phys.* 1995, 193, 89, DOI: 10.1016/0301-0104(94)00415-7
24. Talipov, M. R.; Navale, T. S.; Hossain, M. M.; Shukla, R.; Ivanov, M. V.; Rathore, R. *Angew. Chem.* 2017, 129, 272, DOI: 10.1002/ange.201609695
25. Talipov, M. R.; Boddeda, A.; Timerghazin, Q. K.; Rathore, R. *J. Phys. Chem. C* 2014, 118, 21400, DOI: 10.1021/jp5082752
26. King, B. T.; Kroulík, J.; Robertson, C. R.; Rempala, P.; Hilton, C. L.; Korinek, J. D.; Gortari, L. M. *J. Org. Chem.* 2007, 72, 2279, DOI: 10.1021/jo061515x
27. Zhai, L.; Shukla, R.; Wadumethrige, S. H.; Rathore, R. *J. Org. Chem.* 2010, 75, 4748, DOI: 10.1021/jo100611k
28. Brunschwig, B. S.; Creutz, C.; Sutin, N. *Chem. Soc. Rev.* 2002, 31, 168, DOI: 10.1039/b008034i
29. Ivanov, M.; Talipov, M.; Navale, T.; Rathore, R. *J. Phys. Chem. C* 2018, 122, 2539, DOI: 10.1021/acs.jpcc.7b11232
30. Reed, A. E.; Weinstock, R. B.; Weinhold, F. *J. Chem. Phys.* 1985, 83, 735, DOI: 10.1063/1.449486
31. Hückel, E. *Eur. Phys. J. A* 1932, 76, 628, DOI: 10.1007/BF01341936
32. Hermann, G.; Pohl, V.; Tremblay, J. C.; Paulus, B.; Hege, H.-C.; Schild, A. *J. Comput. Chem.* 2016, 37, 1511, DOI: 10.1002/jcc.24358
33. Mulliken, R. S. *J. Chim. Phys. Phys.-Chim. Biol.* 1949, 46, 497, DOI: 10.1051/jcp/1949460497
34. Wolfsberg, M. A. X.; Helmholz, L. *J. Chem. Phys.* 1952, 20, 837, DOI: 10.1063/1.1700580
35. Hoffmann, R. *J. Chem. Phys.* 1963, 39, 1397, DOI: 10.1063/1.1734456
36. Lu, D.; Zhuang, G.; Wu, H.; Wang, S.; Yang, S.; Du, P. *Angew. Chem., Int. Ed.* 2017, 56, 158, DOI: 10.1002/anie.201608963
37. Wu, J.; Watson, M. D.; Tchegotareva, N.; Wang, Z.; Müllen, K. *J. Org. Chem.* 2004, 69, 8194, DOI: 10.1021/jo0490301
38. Goldsmith, R. H.; Sinks, L. E.; Kelley, R. F.; Betzen, L. J.; Liu, W.; Weiss, E. A.; Ratner, M. A.; Wasielewski, M. R. *Proc. Natl. Acad. Sci. U. S. A.* 2005, 102, 3540, DOI: 10.1073/pnas.0408940102

39. Smith, C. E.; Odoh, S. O.; Ghosh, S.; Gagliardi, L.; Cramer, C. J.; Frisbie, C. D. *J. Am. Chem. Soc.* 2015, 137, 15732, DOI: 10.1021/jacs.5b07400
40. Walther, M. E.; Wenger, O. S. *ChemPhysChem* 2009, 10, 1203, DOI: 10.1002/cphc.200900163
41. Davis, W. B.; Ratner, M. A.; Wasielewski, M. R. *J. Am. Chem. Soc.* 2001, 123, 7877, DOI: 10.1021/ja010330z
42. Franco, C.; Burrezo, P. M.; Lloveras, V.; Caballero, R.; Alcon, I.; Bromley, S. T.; Mas-Torrent, M.; Langa, F.; López Navarrete, J. T.; Rovira, C.; Casado, J.; Veciana, J. *J. Am. Chem. Soc.* 2017, 139, 686, DOI: 10.1021/jacs.6b08649